Civil Engineering and Applied Solutions

Research Article

journal homepage: ceas.journals.umz.ac.ir

CEAS Civil Engineering and Applied Solutions

Comparison of Numerical Performance of a Modified MPS Method with a Least Squares Method Based on a Mixed Formulation for Elasticity Problems

Gholamreza Shobeyri [a*]

[a] *Faculty of Civil, Water & Environmental Engineering, Shahid Beheshti University, Tehran, Iran*

ARTICLE INFO

Article history:

Received 28 April 2026

Revised 30 May 2026

Accepted 16 June 2026

Available online 01 April 2027

Keywords:

Meshless methods

Improved MPS gradient model

Mixed formulation

Least squares method

Elasticity problems

ABSTRACT

High-precision stress analysis of structures under external loading represents a challenge in civil engineering. Although meshless numerical methods show great potential for solving such problems, their early versions often failed to provide acceptable accuracy. A conventional approach to addressing this is the use of a mixed formulation, which transforms second-order governing differential equations into a system of first-order equations. In this approach, both displacements and structural stresses are treated as unknowns. In contrast, in the original second-order formulation, only displacements are unknowns, and stresses are typically derived indirectly from displacement fields, often resulting in low accuracy. This research compares the numerical performance of an improved MPS gradient model by Shobeyri (2023), a well-known meshless method, for stress calculation via second-order equations with a mixed formulation coupled with a least-squares method. The comparison is conducted on two benchmark elasticity problems. The numerical findings reveal that the improved MPS method provides superior stress accuracy. These results suggest that solving the original second-order differential equations, followed by high-precision stress computation, offers a more effective alternative to the mixed formulation approach.

How to cite this article: Shobeyri, G. Comparison of Numerical Performance of a Modified MPS Method with a Least Squares Method Based on a Mixed Formulation for Elasticity Problems. Civil Engineering and Applied Solutions. 2027; 3(2): 26–36. doi:10.22080/ceas.2026.31619.1095.

1. Introduction

In recent years, numerical methods have emerged as a significant tool for solving complex and practical differential equations within engineering fields. Broadly speaking, these methods are categorized into two main groups: mesh-based and meshless methods. Mesh-based methods, which possess a longer historical background, involve the discretization of the computational domain and the approximation of functions and their derivatives through meshing. However, since meshing is generally a computationally expensive and time-consuming process, meshless methods have been developed. These methods enable the solution of differential equations without the need for any underlying mesh, a characteristic that has led to their widespread adoption and significant development.

Although mesh-based numerical methods are still widely used [1-8], efficient meshless numerical methods have also been developed to solve various engineering problems. Among these methods, the Moving Particle Semi-implicit (MPS) method has gained significant attention, leading to the introduction of various modified versions. In this approach, functions and their derivatives are approximated via interpolation functions based on a series of scattered nodes used for domain discretization. This characteristic facilitates the analysis of problems involving complex geometries.

Various problems in solid and fluid mechanics - such as free surface flows [9-11], convective heat transfer [12], multiphase flows [13], fluid-structure interaction [14], the behavior of a molten jet impinging onto a solid plate [15], progressive water waves

* Corresponding author.
E-mail addresses: g_shobeyri@sbu.ac.ir (G. Shobeyri).

https://doi.org/10.22080/ceas.2026.31619.1095
ISSN: 3092-7749/© 2027 The Author(s). Published by University of Mazandaran.

[16], dynamic pressure in dam-break flows [17], two-dimensional hydroelastic slamming [18], fluid lubrication [19], floating structures in waves [20], solid particle dynamics [21], and dense granular flows [22] - have been successfully simulated using the MPS method and its variants. Given the method's inherent capabilities, several techniques have been developed to enhance its performance, most notably those presented in [23-29]. Furthermore, due to the significance of elasticity problems in civil engineering, various meshless numerical methods, such as the Finite Point Method [30], MLPG [31], DLSM [32, 33], and SPH [34] have been employed in numerous studies to analyze such phenomena.

In elasticity problems, once the second-order differential equations - treating structural displacements as unknowns - are solved, the corresponding stresses are typically calculated using numerical methods based on the related formulas. Numerical studies have shown that this approach may lead to reduced accuracy in stress calculation. As an efficient alternative, the second-order differential equations of elasticity can be reformulated as a system of first-order equations that include both structural displacements and stresses; this is known as the mixed formulation [35]. The primary advantage of this formulation is the direct treatment of stresses as unknowns, which yields higher accuracy. However, a larger coefficient matrix is produced due to the increased number of unknowns, leading to a significant increase in computational cost. Despite this, due to its acceptable performance, the mixed formulation has also been applied to various other problems, such as quadratic partial differential equations and free surface problems [36, 37].

This study evaluates the numerical accuracy of a modified MPS gradient model [38] in computing structural stresses via second-order differential equations, comparing it with a mixed formulation coupled with a least-squares method. The investigation is conducted using two benchmark elasticity problems. The results demonstrate that the indirect stress calculation approach, utilizing high-precision numerical methods such as the proposed MPS model, yields superior accuracy compared to the direct stress computation employed in the mixed formulation.

2. The governing equations of elasticity problems

The governing equations for two-dimensional elasticity problems are expressed by Eqs. 1 and 2 [39].

$$(\lambda+2\mu)\frac{\partial^2 u_x}{\partial x^2}+\mu\frac{\partial^2 u_x}{\partial y^2}+(\lambda+\mu)\frac{\partial^2 u_y}{\partial x\partial y}=-fr_x \tag{1}$$

$$\mu\frac{\partial^2 u_y}{\partial x^2}+(\lambda+2\mu)\frac{\partial^2 u_y}{\partial y^2}+(\lambda+\mu)\frac{\partial^2 u_x}{\partial x\partial y}=-fr_y \tag{2}$$

where u_x and u_y represent the horizontal and vertical displacements, respectively, and fr_x and fr_y denote the external forces in the x and y directions. ∂^2 is also the second-order partial derivative operator. The Lamé constants, λ and μ, are defined by Eq. 3.

$$\mu=\frac{E}{2(1+\nu)}>0,\ \ \lambda=\frac{E\nu}{(1-2\nu)(1+\nu)}>0 \tag{3}$$

where ν is the Poisson's ratio and E is the Young's modulus.

In the mixed formulation, a system of first-order equations comprising displacements and stresses (Eqs. 4a to 4e) is employed as an alternative to the second-order differential Eqs. 1 and 2 [35].

$$\frac{\partial\sigma_{xx}}{\partial x}+\frac{\partial\tau_{xy}}{\partial y}=-fr_x \tag{4a}$$

$$\frac{\partial\tau_{xy}}{\partial x}+\frac{\partial\sigma_{yy}}{\partial y}=-fr_y \tag{4b}$$

$$\sigma_{xx}=(\lambda+2\mu)\frac{\partial u_x}{\partial x}+\lambda\frac{\partial u_y}{\partial y} \tag{4c}$$

$$\sigma_{yy}=\lambda\frac{\partial u_x}{\partial x}+(\lambda+2\mu)\frac{\partial u_y}{\partial y} \tag{4d}$$

$$\tau_{xy}=\mu(\frac{\partial u_x}{\partial y}+\frac{\partial u_y}{\partial x}) \tag{4e}$$

where σ_{xx} and σ_{yy} denote the normal stresses and τ_{xy} represents the shear (tangential) stress. The compact form of these equations is given by Eq. 5.

$$L(\varphi)+F=0 \tag{5}$$

where $L(.)$ is a first-order differential operator, defined by Eq. 6.

$$L(.)=L_1(.)_x+L_2(.)_y+L_3(.) \tag{6}$$

The vector of unknowns, φ, is given by Eq. 7.

$$\varphi=\left[u_x,u_y,\sigma_{xx},\sigma_{yy},\tau_{xy}\right]^T \tag{7}$$

The vector F is similarly defined by Eq. 8.

$$F = \left[0,0,0,\text{-}fr_x,\text{-}fr_y\right]^T \tag{8}$$

The operators $L_1(.)_x$, $L_2(.)_y$ and $L_3(.)$ can be expressed by Eq. 9.

$$L_1 = \begin{bmatrix} \lambda+2\mu & 0 & 0 & 0 & 0 \\ \lambda & 0 & 0 & 0 & 0 \\ 0 & \mu & 0 & 0 & 0 \\ 0 & 0 & 1 & 0 & 0 \\ 0 & 0 & 0 & 0 & 1 \end{bmatrix},\ L_2 = \begin{bmatrix} 0 & \lambda & 0 & 0 & 0 \\ 0 & \lambda+2\mu & 0 & 0 & 0 \\ \mu & 0 & 0 & 0 & 0 \\ 0 & 0 & 0 & 0 & 1 \\ 0 & 0 & 0 & 1 & 0 \end{bmatrix},\ L_3 = \begin{bmatrix} 0 & 0 & -1 & 0 & 0 \\ 0 & 0 & 0 & -1 & 0 \\ 0 & 0 & 0 & 0 & -1 \\ 0 & 0 & 0 & 0 & 0 \\ 0 & 0 & 0 & 0 & 0 \end{bmatrix} \tag{9}$$

3. Numerical methods

3.1. Improved MPS gradient model

In the MPS method, the gradient and Laplacian operators of an arbitrary function f are approximated in two dimensions using a weighted averaging approach [9] as shown in Eqs. 10 and 11.

$$\nabla f_i = \sum_{j\neq i} \frac{2}{n_j} \frac{f_j - f_i}{|\mathbf{r}_j - \mathbf{r}_i|^2} (\mathbf{r}_j - \mathbf{r}_i) W(|\mathbf{r}_j - \mathbf{r}_i|, R_s) \tag{10}$$

$$\nabla^2 f_i = \frac{4}{\lambda} \sum_{j\neq i} \frac{1}{n_j} (f_j - f_i) W(|\mathbf{r}_j - \mathbf{r}_i|, R_s) \tag{11}$$

where i denotes the reference node, while j represents its neighboring nodes. Furthermore, r and $W(|\mathbf{r}_j - \mathbf{r}_i|, R_s)$ or $W(|\mathbf{r}_j - \mathbf{r}_i|)$ denote the relative position vector and the interpolation function, respectively. The computational parameters n_j and λ are defined by Eqs. 12 and 13.

$$n_i = \sum_{j\neq i} W(|\mathbf{r}_j - \mathbf{r}_i|, R_s) \tag{12}$$

$$\lambda = \frac{\int_\Omega W(r)\, r^2\, d\Omega}{\int_\Omega W(r) d\Omega} \tag{13}$$

where Ω is the interaction area of node i and $r = |\mathbf{r}_j - \mathbf{r}_i|$.

One of the most efficient interpolation functions is expressed by Eq. 14.

$$W(r, R_s) = \frac{8}{\pi R_s^2} \left[\frac{3}{4}\left(\frac{r}{R_s}\right)^2 - \frac{3}{2}\left(\frac{r}{R_s}\right) + \frac{3}{4}\right] \tag{14}$$

where R_s denotes the size of the interaction area for the reference node.

An improved MPS gradient model, characterized by remarkable numerical performance, is proposed in Eq. 15.

$$\nabla f_i = \left[\frac{1}{\lambda} \sum_{j\neq i} \frac{1}{n_j} W(|\mathbf{r}_j - \mathbf{r}_i|) (\mathbf{r}_j - \mathbf{r}_i) \otimes (\mathbf{r}_j - \mathbf{r}_i)^T\right]^{-1} \left[\frac{1}{\lambda} \sum_{j\neq i} \frac{1}{n_j} W(|\mathbf{r}_j - \mathbf{r}_i|)(f_j - f_i)(\mathbf{r}_j - \mathbf{r}_i)\right] \tag{15}$$

This model has been successfully applied to achieve non-oscillatory stress calculations in elasticity problems. Detailed formulations of this gradient model, including the derivation of second-order derivatives required for Eqs. 1 and 2 via the MPS method, are provided in reference [38].

3.2. The least square scheme in the mixed formulation

The first-order Taylor series expansion for a function f around a central node with position (x_0, y_0) is given by Eq. 16.

$$f(x, y) \approx f_0 + \frac{\partial f_0}{\partial x} \Delta x + \frac{\partial f_0}{\partial y} \Delta y \tag{16}$$

where $\Delta x = x - x_0$ and $\Delta y = y - y_0$.

By applying this expansion to all computational nodes within the interaction area of the reference node, we obtain Eq. 17.

$$\begin{bmatrix} 1 & \Delta x_1 & \Delta y_1 \\ 1 & \Delta x_2 & \Delta y_2 \\ \cdots & \cdots & \cdots \\ 1 & \Delta x_N & \Delta y_N \end{bmatrix} \begin{bmatrix} f_0 \\ \partial f_0/\partial x \\ \partial f_0/\partial y \end{bmatrix} = \begin{bmatrix} f_1 \\ f_2 \\ \cdots \\ f_N \end{bmatrix} \tag{17}$$

where N denotes the total number of surrounding nodes.

Solving this system allows for the determination of the approximated function values at the computational nodes $(f_1, f_2, \ldots, f_N)$. The total approximation error, $\|E\|$, is expressed by Eq. 18.

$$\|E\| = \sum_{j=1}^{N}\left[f_0 - f_j + \frac{\partial f_0}{\partial x}\Delta x_j + \frac{\partial f_0}{\partial y}\Delta y_j\right]^2 W_j^2 \tag{18}$$

where W_j is the value of the interpolation function at node j.

By minimizing this error function using a weighted least-squares scheme, the vector of unknown parameters can be calculated as shown in Eqs. 19 and 20.

$$\frac{\partial\|E\|}{\partial F} = 0 \tag{19}$$

$$\begin{bmatrix} f_0 \\ \partial f_0/\partial x \\ \partial f_0/\partial y \end{bmatrix} = \begin{bmatrix} \sum W_j^2 & \sum W_j^2\Delta x_j & \sum W_j^2\Delta y_j \\ \sum W_j^2\Delta x_j & \sum W_j^2\Delta x_j^2 & \sum W_j^2\Delta x_j\Delta y_j \\ \sum W_j^2\Delta y_j & \sum W_j^2\Delta x_j\Delta y_j & \sum W_j^2\Delta y_j^2 \end{bmatrix}^{-1} \begin{pmatrix} \sum f_j W_j^2 \\ \sum f_j W_j^2\Delta x_j \\ \sum f_j W_j^2\Delta y_j \end{pmatrix} \tag{20}$$

where $F = [f_0, \partial f_0/\partial x\,, \partial f_0/\partial y]$ contains the unknown values of the function and its derivatives at the reference node. The interpolation function for this method is defined by Eq. 21.

$$W(r) = \begin{cases} \frac{1}{r^3+\eta^3} & r \le R_s \\ 0 & r > R_s \end{cases} \tag{21}$$

In this study, the average nodal distance (defined later as l_0) is chosen for the parameter η (as a small value) in Eq. 21 to prevent a zero denominator. A similar least-squares method, based on a second-order Taylor expansion, has been employed to solve free-surface and elasticity problems, as well as elliptic PDEs [40-42].

By approximating the function and its first-order derivatives at all computational nodes, the system of first-order equations (Eqs. 4a and 4e) can be solved to obtain the unknown variables of the elasticity problem (displacements and stresses) in the mixed formulation. This system of equations is solvable by applying the boundary conditions using the known analytical results. One advantage of the mixed formulation is that stresses can be calculated directly with lower errors. Conversely, stresses can also be calculated after determining the displacements from the second-order differential equations (Eqs. 1 and 2) by using the Eqs. 4c and 4e; however, this approach may lead to larger errors.

4. Numerical examples

4.1. Cantilever beam

To compare the performance of these two numerical methods, a cantilever beam subjected to a load at its free end is examined in the first numerical example, with the initial geometry illustrated in Fig. 1. The analytical solutions for the displacements and stresses ($u_x, u_y, \sigma_{xx}, \sigma_{yy}, \tau_{xy}$) are provided in [39]. Applying the governing differential equations to the internal nodes results in a non-square matrix. However, by incorporating the analytical solutions of the boundary nodes into the right-hand side (RHS) vector, a square system of equations is obtained, the solution of which yields the unknowns at the internal nodes. It is worth noting that the final system of equations resulting from the discretization of the differential equations was solved using Gaussian elimination. The computational constants $P = 1, E = 10000, c = 1, L = 16$ and $\nu = 0.25$ (in SI units) are used for this test problem.

The computational nodes are initially placed at the vertices of a square grid with a spacing of l_0 and are subsequently moved randomly with a maximum displacement of kl_0, where k is the randomness coefficient. To solve the problem, this coefficient is set to 0.25, and three irregular node distributions with $l_0 = 1/2, 1/4, 1/6$ m are applied (see Fig. 2 with $l_0 = 1/6$ m).

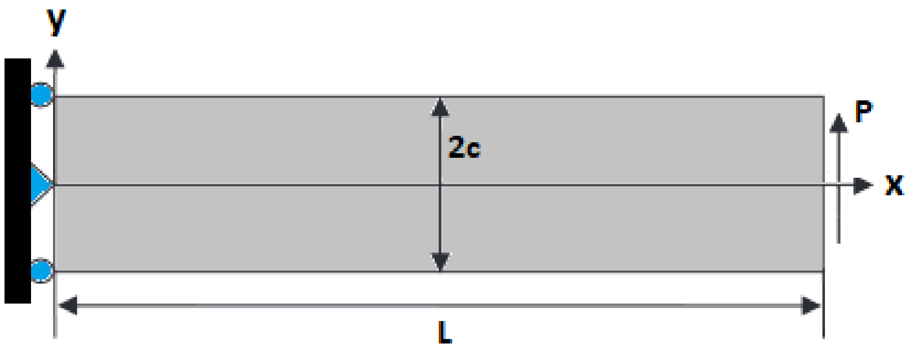

Fig. 1. The Initial geometry of the cantilever beam problem.

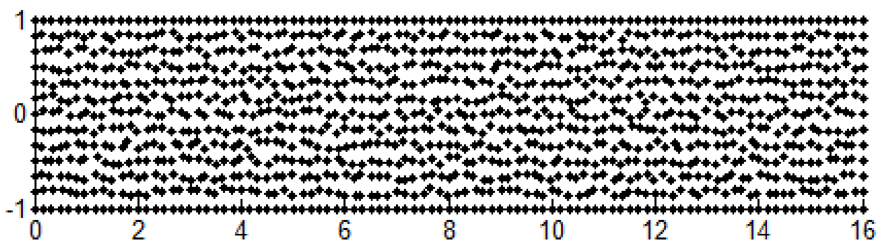

Fig. 2. The nodal distribution with $l_0 = 1/6$ m for the cantilever beam problem.

In this research, Eq. 22 is employed to evaluate the error of the numerical methods in solving this problem.

$$Er_1 = \frac{\Sigma(f_i - \bar{f}_i)^2}{Nb(min(\bar{f}))^2} \tag{22}$$

In Eq. 22, f_i and $\bar{f}_i$ represent the numerical and analytical values of the normal stress (σ_{xx}) at the nodes on the upper face of the beam, respectively. Additionally, $min(\bar{f})$ and Nb denote the minimum value and the total number of computational nodes on this face, respectively.

The computational errors for both numerical methods and the utilized nodal distributions are shown in Fig. 3, according to the defined error indicator. As observed, the improved MPS model offers higher accuracy than the mixed method.

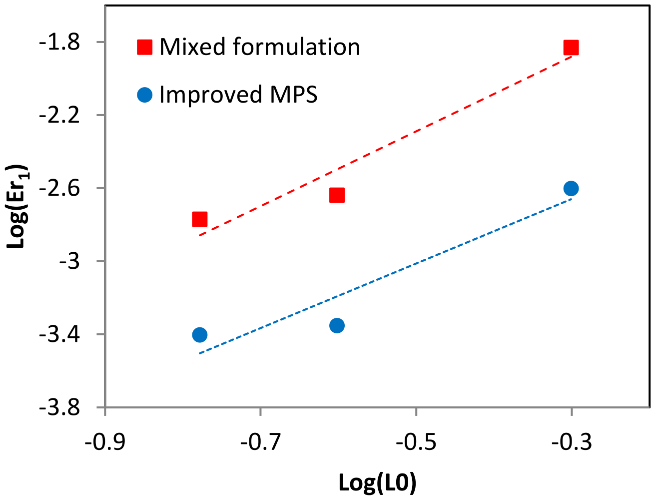

Fig. 3. Error analysis of the numerical methods for the cantilever beam problem.

Fig. 4 illustrates a comparison between the calculated normal stress (σ_{xx}) along the beam's upper edge and the corresponding analytical results. While the MPS method yields results of acceptable accuracy, the mixed formulation exhibits significant fluctuations, thereby highlighting the superiority of the MPS approach. Notably, despite the mixed formulation's ability to solve for stresses directly as primary unknowns, the MPS method provides more consistent and promising results.

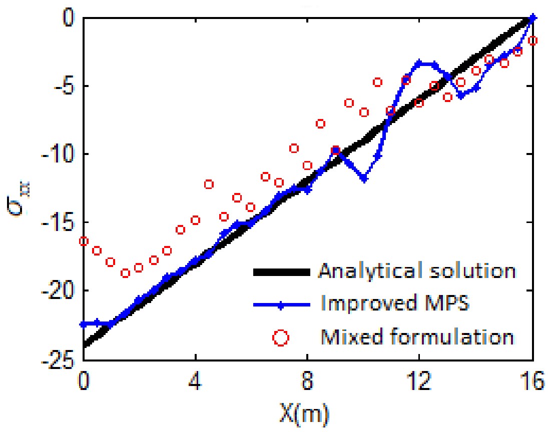

(a)

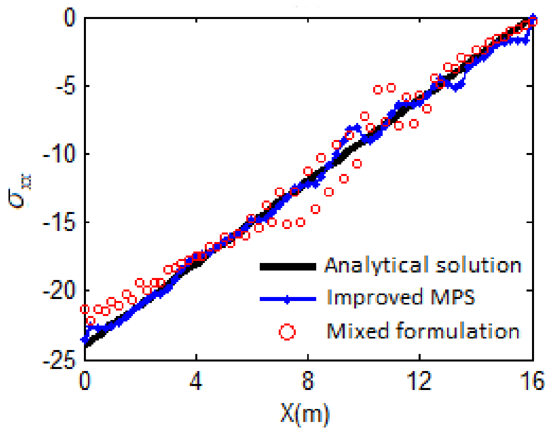

(b)

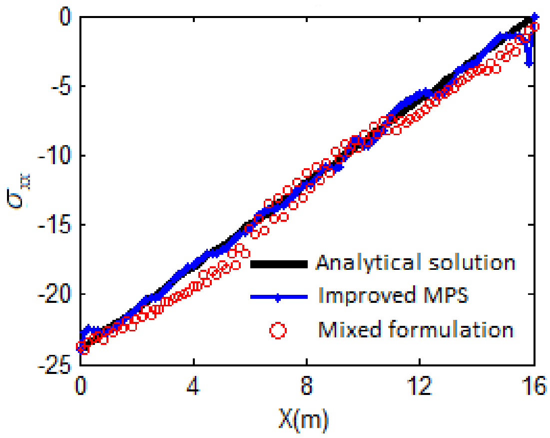

(c)

Fig. 4. Comparison of computational and analytical results of stress at the top of the beam for: (a) $l_0 = 1/2$ m; (b) $l_0 = 1/4$ m; and (c) $l_0 = 1/6$ m.

The results of meshless numerical methods are highly dependent on the size of the interaction area. In this study, the optimal value of this parameter is selected such that the defined numerical error (Eq. 22) is minimized. It is evident that the optimal size of R_s differs for the two numerical methods, as presented in Fig. 5. As evident, the MPS method requires a significantly larger R_s for the finest node distribution compared to the mixed method to achieve minimum error, thereby increasing the computational cost (the processor is Intel Core i5, CPU@2.00 GHz-2.6 GHz, and RAM 4.00 GB). Conversely, the larger system of equations in the mixed method also incurs high computational expenses.

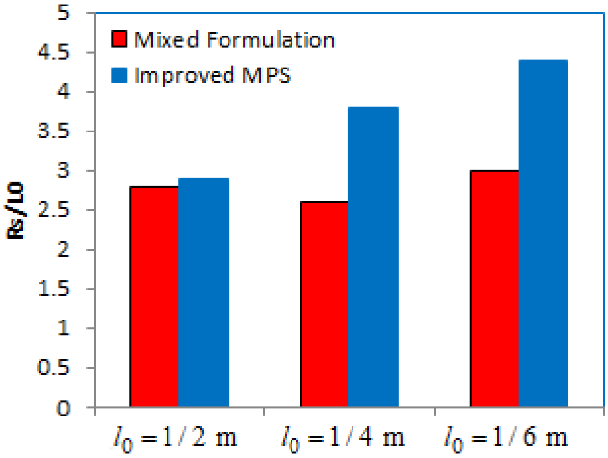

Fig. 5. Optimal values of R_s for the cantilever beam problem.

Under these conditions, the MPS method is only moderately more time-consuming for this specific nodal distribution. For the other two nodal distributions, both methods require approximately the same computational time (see Fig. 6). Fig. 7 illustrates the error variations for different R_s values and the nodal distributions. It is evident that the improved MPS method exhibits less sensitivity to changes in this parameter compared to the mixed method. In other words, reducing the R_s value in the MPS scheme does not lead to a significant decrease in accuracy, but rather considerably reduces the computational cost. Considering both the accuracy of the results and the computational cost simultaneously, the MPS method can be regarded as more efficient.

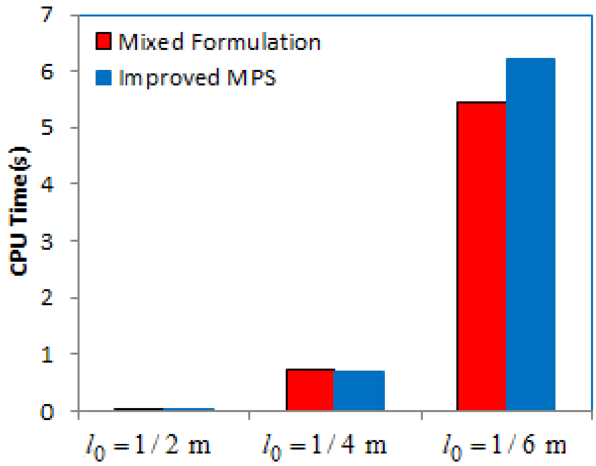

Fig. 6. Computational times of the numerical methods for the cantilever beam problem.

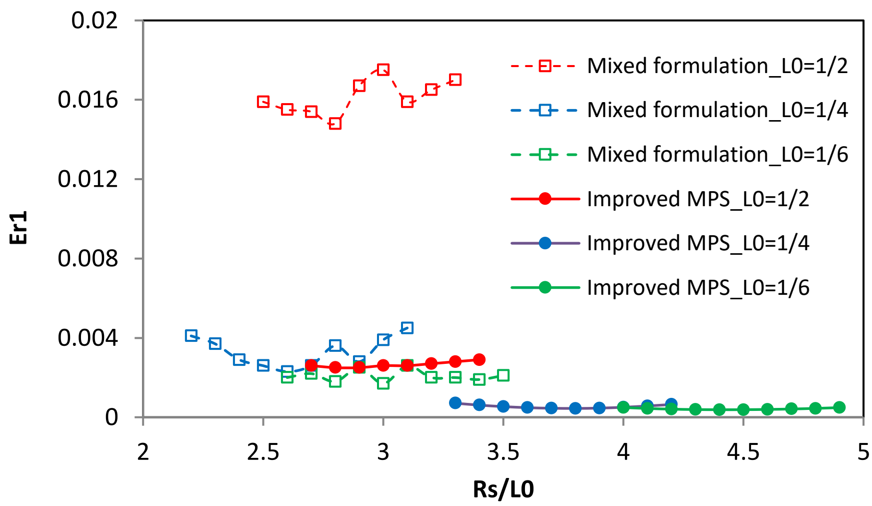

Fig. 7. Variation of numerical error for different R_s values in the cantilever beam problem.

To further evaluate the numerical performance of these two methods under more complex conditions, a highly irregular nodal distribution ($k = 0.5$) with $l_0 = 1/6$ m was employed. As illustrated in Fig. 8, the improved MPS method exhibits significantly lower fluctuations in the calculated normal stress (σ_{xx}) at the upper part of the beam compared to the mixed formulation. This demonstrates the robustness of the proposed method, even when applied to highly irregular nodal distributions. To reduce computational costs for a fixed number of nodes, these nodes can be distributed such that a higher density is placed in regions with higher errors.

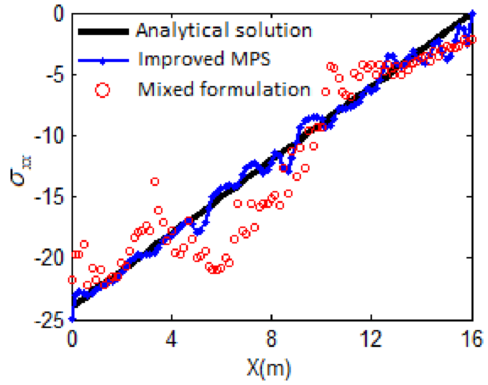

Fig. 8. Comparison of the computational and analytical results of stress at the top of the beam for highly irregular nodal distribution with $k = 0.5$ using $l_0 = 1/6$ m.

This process results in a refined nodal distribution, which is essential for achieving high accuracy in complex conditions. As shown in Fig. 9, two different refined nodal patterns, corresponding to $l_0 = 1/6$ m and $k = 0.15$, are employed to compare the numerical methods investigated in this study. Fig. 10 illustrates the calculated normal stress along the upper edge of the beam for the distributions shown in Fig. 9; these results reaffirm the superior accuracy of the improved MPS model compared to the mixed method. It should be noted that the nodal distribution in Fig. 9b was intentionally chosen with high irregularity to further demonstrate the remarkable capabilities of the MPS method. Consequently, the mixed method exhibits significant oscillations under such conditions. However, when a distribution with lower irregularity is employed, such as the one shown in Fig. 9a, the mixed method yields results with considerably fewer oscillations.

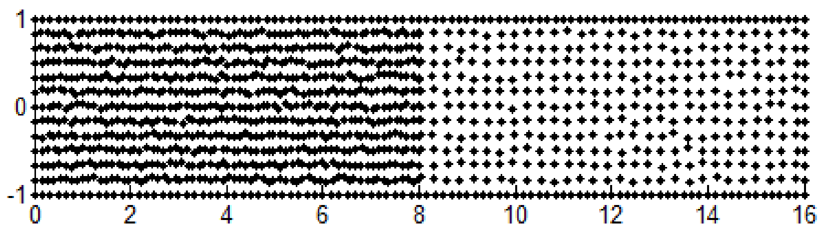

(a)

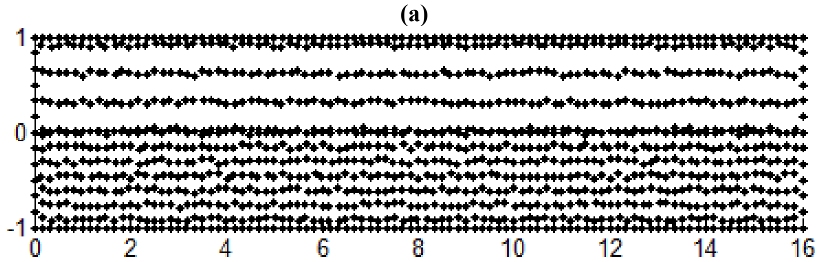

(b)

Fig. 9. Two refined nodal distributions with different patterns with $l_0 = 1/6$ m and $k = 0.15$ for the solution of the cantilever beam problem: (a) first pattern; and (b) second pattern.

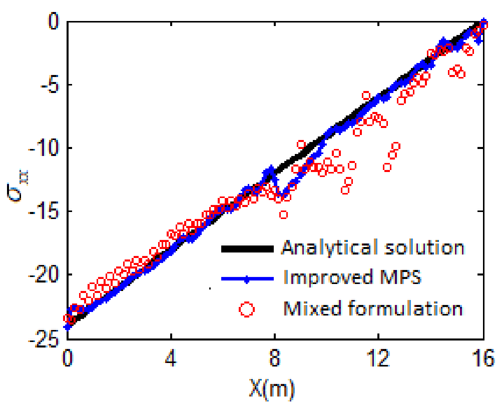

(a)

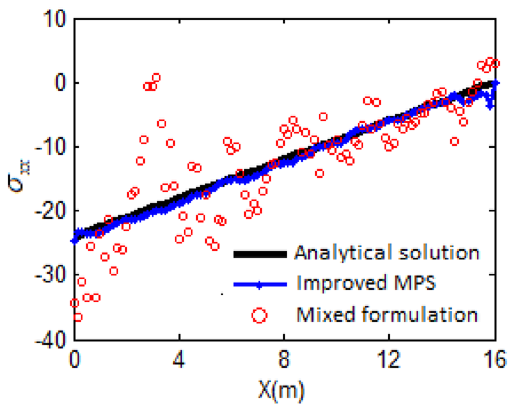

(b)

Fig. 10 Comparison of the computational and analytical results of stress at the top of the beam corresponding to the refined nodal distributions shown in Fig. 9: (a) results corresponding to Fig. 9a; and (b) results corresponding to Fig. 9b.

4.2. *Infinite plate with a circular hole*

The second benchmark problem in this study is an infinite plate containing a circular hole under uniaxial tension, with the geometry shown in Fig. 11. The analytical solutions for the displacements and stresses of this problem are provided in [39]. Due to the symmetry of the problem, a square domain in the first quadrant with a side length of $6a_p$ (where $a_p = 1$ m is the radius of the hole) is considered as the computational domain. The following constants (in SI units) are applied to solve this test problem: $P = 1$, $E = 1000$ and $\nu = 0.3$.

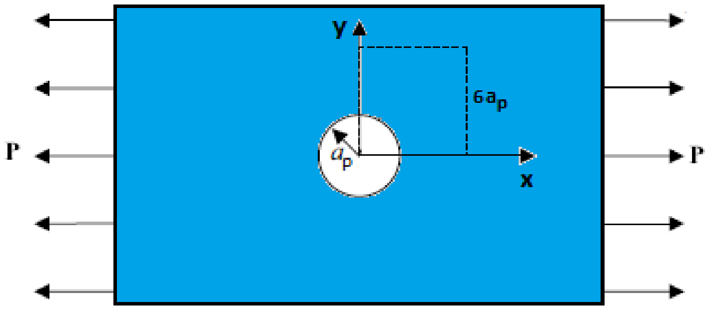

Fig. 11. The geometry of an infinite plate with a circular hole subjected to a uniaxial load.

The error indicator for this problem is given by Eq. 23.

$$Er_2 = \frac{\Sigma(g_i - \bar{g}_i)^2}{Nh(max(\bar{g}))^2} \tag{23}$$

In Eq. 23, g_i and $\bar{g}_i$ represent the numerical and analytical values of the normal stress σ_{xx} at the nodes along the left edge of the plate, respectively. Additionally, $max(\bar{g})$ and Nh denote the maximum value and the total number of computational nodes on the edge, respectively.

An irregular nodal distribution with $l_0 = 1/6$ m and $k = 0.3$ as shown in Fig. 12 is used to solve this problem. In Fig. 13, the calculated normal stresses (σ_{xx}) along the left edge of the plate ($x = 0$ m) are compared with the analytical solution, demonstrating the superior accuracy of the improved MPS model. It is worth noting that the best results are obtained based on the error indicator defined in Eq. 23. Additionally, the performance of the numerical methods for the refined nodal distribution shown in Fig. 14 ($l_0 = 1/6$ m, $k = 0.3$) is presented in Fig. 15. As is evident, the MPS method once again proves its ability to produce results with high accuracy, whereas the mixed method yields fluctuating results.

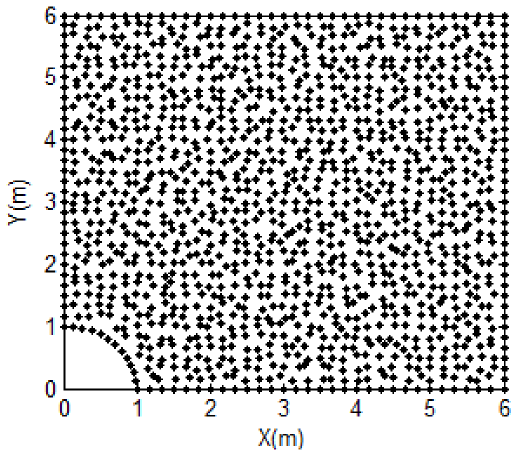

Fig. 12. The nodal distribution with $l_0 = 1/6$ m and $k = 0.3$ for the plate problem.

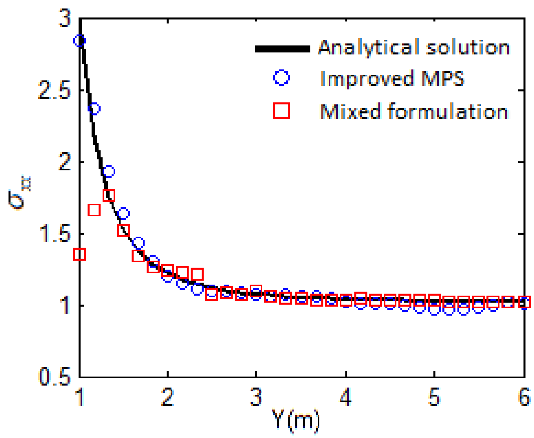

Fig. 13. Comparison of the computational and analytical results of stress along the left edge of the plate.

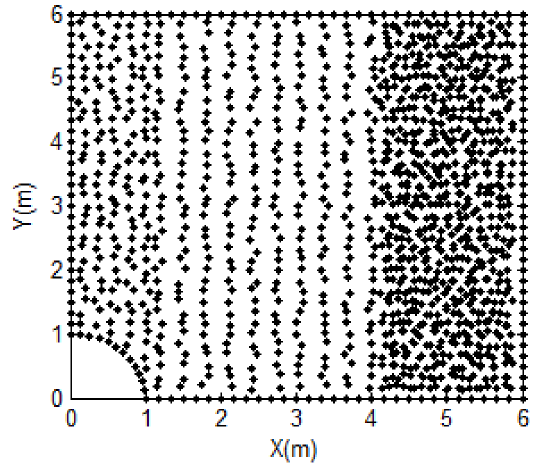

Fig. 14. The refined nodal distribution with $l_0 = 1/6$ m and $k = 0.3$ for the solution of the plate problem.

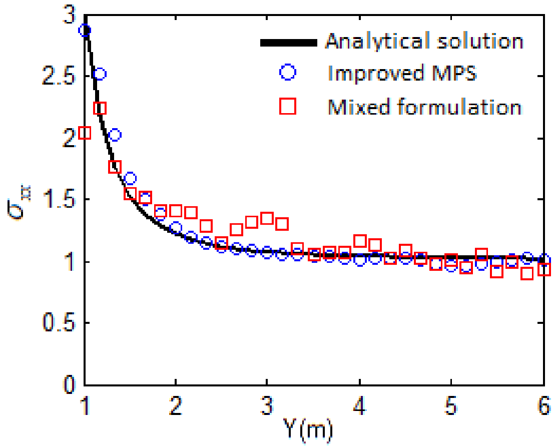

Fig. 15. Comparison of the computational and analytical results of stress at the left edge of the plate for the refined nodal distributions of Fig. 14.

5. Conclusions

This study evaluated the accuracy of stress estimation using numerical methods for two benchmark elasticity problems. In the first approach, the second-order governing differential equations, with structural displacements as the primary unknowns, were solved using the MPS method. The corresponding stresses were subsequently derived through the existing displacement-stress relationships and a modified MPS gradient model [38]. In the second approach, the second-order equations were reformulated into a mixed formulation comprising a system of first-order differential equations, where both displacements and stresses were treated as unknowns and solved via a least-squares method. Based on the obtained numerical results, the following key observations can be drawn:

- The indirect determination of stresses using the modified MPS gradient model (Method 1) yields results with lower error compared to the mixed method (Method 2).
- The results of Method 1 exhibit less sensitivity to variations in the size of the interaction area.
- The accuracy of Method 1 is relatively insensitive to the increasing irregularity of the computational node distribution, whereas Method 2 exhibits greater sensitivity to this factor.
- Method 1 exhibits superior numerical performance for the refined node distributions.
- Considering both accuracy and computational cost simultaneously, it can be concluded that Method 1 is more efficient.

These findings serve as a guide for selecting appropriate numerical methods to achieve high-precision stress analysis in complex, real-world structural problems.

Statements & declarations

Author contributions

Gholamreza Shobeyri: Conceptualization, Methodology, Numerical analysis, Writing - Original Draft, Writing - Review & Editing.

Funding

The author received no financial support for the research, authorship, and/or publication of this manuscript.

Data availability

The data presented in this study will be available on interested request from the corresponding author.

Declarations

The author declares no conflict of interest.

References

[1] Jebalbarezi Sarbijan, M., Shirini, B., Rooholamini, H. Investigation of Crack Growth Behavior in Heterogeneous Asphalt Concrete Using FEM Modeling Based on Random Aggregate Generation and Distribution Algorithms. Civil Engineering and Applied Solutions, 2026; 2: 46–57. doi:10.22080/ceas.2025.29529.1020.

[2] Sadeghi, V., Bagheri, M., Abasi Hamidi, J. Earthquake-Induced Deformation of Road Embankments: A Finite Difference Method. Civil Engineering and Applied Solutions, 2026; 2: 28–41. doi:10.22080/ceas.2026.30800.1066.

[3] Ghaseminejad, V., Moosavi, S. M., Zargar Herijani, T. Parametric Study of Settlement in Shallow Foundations of Adjacent Buildings on Sandy Soil: A Finite Element Parametric Study. Civil Engineering and Applied Solutions, 2026; 2: 73–84. doi:10.22080/ceas.2026.30450.1053.

[4] Ansari, B., Moazzami, A. Soil Freezing Model in the Presence of Underground Inclusion Using Hybrid Boundary-Finite Element Method. Numerical Methods in Civil Engineering, 2026; 10: 25–41. doi:10.61882/NMCE.2511.1107.

[5] Shafiee, A. H., Oulapour, M., Shlaka Drifesh, Z. Uplift Capacity of Granular Pile Anchors in Clay Using Finite Element Limit Analysis. Numerical Methods in Civil Engineering, 2025; 9: 1–8. doi:10.61186/NMCE.2409.1074.

[6] Asadi, R., Zamani Aliabadi, Z. Comparison of numerical methods for the solution of Richards' equation in layered porous media. Numerical Methods in Civil Engineering, 2025; 9: 1–10. doi:10.61186/NMCE.2302.1007.

[7] Daliri, M., Ghohani Arab, H., Miri, M., Khatibi, S. H. Prediction of Shear Strength in SCS Panels with One-End Welded BP Shear Connector Using Numerical Modeling and Gene Expression Programming (GEP). AUT Journal of Civil Engineering, 2025; 9: 185–204. doi:10.22060/ajce.2025.23945.5907.

[8] Kiani Fordoei, M. A., Khodaparast, M., Ghadamgahi, A. Numerical investigation of behavior of energy piles in saturated fine-grained soil. AUT Journal of Civil Engineering, 2024; 8: 145–160. doi:10.22060/ajce.2025.23636.5891.

[9] Koshizuka, S., Oka, Y. Moving-Particle Semi-Implicit Method for Fragmentation of Incompressible Fluid. Nuclear Science and Engineering, 1996; 123: 421–434. doi:10.13182/NSE96-A24205.

[10] Ataie-Ashtiani, B., Farhadi, L. A stable moving-particle semi-implicit method for free surface flows. Fluid Dynamics Research, 2006; 38: 241. doi:10.1016/j.fluiddyn.2005.12.002.

[11] Geng, C., Wang, W.-h., Heng, M.-y., Zhao, Y., Yang, H., Huang, Y. A new free surface identification method for 3D MPS method. Scientific Reports, 2026; 16: 13829. doi:10.1038/s41598-026-44218-9.

[12] Zhang, S., Morita, K., Fukuda, K., Shirakawa, N. An improved MPS method for numerical simulations of convective heat transfer problems. International Journal for Numerical Methods in Fluids, 2006; 51: 31–47. doi:10.1002/fld.1106.

[13] Khayyer, A., Gotoh, H. Enhancement of performance and stability of MPS mesh-free particle method for multiphase flows characterized by high density ratios. Journal of Computational Physics, 2013; 242: 211–233. doi:10.1016/j.jcp.2013.02.002.

[14] Sun, Z., Djidjeli, K., Xing, J. T., Cheng, F. Modified MPS method for the 2D fluid structure interaction problem with free surface. Computers & Fluids, 2015; 122: 47–65. doi:10.1016/j.compfluid.2015.08.017.

[15] Li, G., Liu, M., Duan, G., Chong, D., Yan, J. Numerical investigation of erosion and heat transfer characteristics of molten jet impinging onto solid plate with MPS–LES method. International Journal of Heat and Mass Transfer, 2016; 99: 44–52. doi:10.1016/j.ijheatmasstransfer.2016.03.090.

[16] Wang, L., Jiang, Q., Zhang, C. Improvement of moving particle semi-implicit method for simulation of progressive water waves. International Journal for Numerical Methods in Fluids, 2017; 85: 69–89. doi:10.1002/fld.4373.

[17] Wang, L., Jiang, Q., Nie, S., Zhang, J., Iddy, I. Improvement on MPS Method for Simulation of Dynamic Pressure in Dam Break Flows. Journal of Coastal Research, 2018; 85: 971–975. doi:10.2112/SI85-195.1.

[18] Zha, R., Peng, H., Qiu, W. An improved higher-order moving particle semi-implicit method for simulations of two-dimensional hydroelastic slamming. Physics of Fluids, 2021; 33: 037104. doi:10.1063/5.0033491.

[19] Yamada, D., Imatani, T., Shibata, K., Maniwa, K., Obara, S., Negishi, H. Application of improved multiresolution technique for the MPS method to fluid lubrication. Computational Particle Mechanics, 2022; 9: 421–441. doi:10.1007/s40571-021-00420-2.

[20] Zhang, G., Zhao, W., Wan, D. Moving Particle Semi-implicit method coupled with Finite Element Method for hydroelastic responses of floating structures in waves. European Journal of Mechanics - B/Fluids, 2022; 95: 63–82. doi:10.1016/j.euromechflu.2022.04.005.

[21] Kim, K. S. Numerical Modeling of Solid Particle Dynamics Using the Moving Particle Semi-Implicit (MPS) Method in Seabed Penetration Scenarios. Journal of Coastal Research, 2024; 116: 548–552. doi:10.2112/JCR-SI116-111.1.

[22] Mumeen, A., Rufai, O., Jin, Y.-C. MPS simulation of dense granular flows using a gradient-expansion nonlocal μ(I) rheology. Particuology, 2026; 114: 186–206. doi:10.1016/j.partic.2026.04.013.

[23] Khayyer, A., Gotoh, H. A higher order Laplacian model for enhancement and stabilization of pressure calculation by the MPS method. Applied Ocean Research, 2010; 32: 124–131. doi:10.1016/j.apor.2010.01.001.

[24] Tamai, T., Koshizuka, S. Least squares moving particle semi-implicit method. Computational Particle Mechanics, 2014; 1: 277–305. doi:10.1007/s40571-014-0027-2.

[25] Shobeyri, G., Madadi, H. An improvement in MPS method using Voronoi diagram and a new kernel function. Journal of the Brazilian Society of Mechanical Sciences and Engineering, 2018; 40: 172. doi:10.1007/s40430-018-1121-9.

[26] Duan, G., Yamaji, A., Koshizuka, S., Chen, B. The truncation and stabilization error in multiphase moving particle semi-implicit method based on corrective matrix: Which is dominant? Computers & Fluids, 2019; 190: 254–273. doi:10.1016/j.compfluid.2019.06.023.

[27] Li, D., Zhang, H., Qin, G. A Modified MPS Method with a Split-Pressure Poisson Equation and a Virtual Particle for Simulating Free Surface Flows. Journal of Marine Science and Engineering, 2023; 11: 215. doi:10.3390/jmse11010215.

[28] Shobeyri, G. Improved MPS models for simulating free surface flows. Mathematics and Computers in Simulation, 2024; 218: 79–97. doi:10.1016/j.matcom.2023.11.015.

[29] Shobeyri, G. Novel SPH and MPS Laplacian Models Improved by MLS Method for Solving Poisson equations. Numerical Methods in Civil Engineering, 2024; 9: 29–39. doi:10.61186/NMCE.2406.1061.

[30] Oñate, E., Perazzo, F., Miquel, J. A finite point method for elasticity problems. Computers & Structures, 2001; 79: 2151–2163. doi:10.1016/S0045-7949(01)00067-0.

[31] Atluri, S. N., Liu, H. T., Han, Z. D. Meshless Local Petrov-Galerkin (MLPG) Mixed Collocation Method For Elasticity Problems. Computer Modeling in Engineering \& Sciences, 2006; 14: 141–152. doi:10.3970/cmes.2006.014.141.

[32] Afshar, M. H., Amani, J., Naisipour, M. A node enrichment adaptive refinement in Discrete Least Squares Meshless method for solution of elasticity problems. Engineering Analysis with Boundary Elements, 2012; 36: 385–393. doi:10.1016/j.enganabound.2011.08.012.

[33] Nikravesh Kazeroni, S., Afshar, M. H., Faraji, S. RPIM and RPIM-MLS based MDLSM method for the solution of elasticity problems. Scientia Iranica, 2016; 23: 2458–2468. doi:10.24200/sci.2016.2305.

[34] Shobeyri, G. Mixed Smoothed Particle Hydrodynamics Method for Planar Elasticity Problems. Iranian Journal of Science and Technology, Transactions of Civil Engineering, 2023; 47: 491–504. doi:10.1007/s40996-022-00883-0.

[35] Amani, J., Afshar, M. H., Naisipour, M. Mixed discrete least squares meshless method for planar elasticity problems using regular and irregular nodal distributions. Engineering Analysis with Boundary Elements, 2012; 36: 894–902. doi:10.1016/j.enganabound.2011.09.012.

[36] Faraji, S., Afshar, M. H., Amani, J. Mixed discrete least square meshless method for solution of quadratic partial differential equations. Scientia Iranica, 2014; 21: 492–504.

[37] Eini, N., Afshar, M. H., Faraji Gargari, S., Shobeyri, G., Afshar, A. A fully Lagrangian mixed discrete least squares meshfree method for simulating the free surface flow problems. Engineering with Computers, 2022; 38: 331–351. doi:10.1007/s00366-020-01157-x.

[38] Shobeyri, G. Improved MPS Gradient Models for Elasticity Problems. Iranian Journal of Science and Technology, Transactions of Civil Engineering, 2023; 47: 1831–1843. doi:10.1007/s40996-022-01013-6.

[39] Timoshenko, S., Goodier, J. N. Theory of Elasticity. 3rd ed. New York (NY): McGraw Hill; 1987.

[40] Koh, C. G., Gao, M., Luo, C. A new particle method for simulation of incompressible free surface flow problems. International Journal for Numerical Methods in Engineering, 2012; 89: 1582–1604. doi:10.1002/nme.3303.

[41] Shobeyri, G., Najafabadi, S. H. G., Abed, M. A Comparative Study on Two Mixed Least Squares Meshless Models with Improved SPH, MPS and CPM Methods to Solve Elasticity Problems. Iranian Journal of Science and Technology, Transactions of Mechanical Engineering, 2024; 48: 1565–1580. doi:10.1007/s40997-023-00742-x.

[42] Shobeyri, G., Ghoreishi Najafabadi, S. H., Abed, M. Computational efficiency of mixed least squares meshless models over SPH method for elliptic PDEs. AUT Journal of Civil Engineering, 2024; 8: 17–32. doi:10.22060/ajce.2024.22777.5847.